

**Wiley Analytical Science**

# **Wiley Analytical Science Virtual Conference**

**November 9-17**

## **For the 3rd time, The Wiley Analytical Science Conference is back!**

**It's all happening November 9 - 17**

The Wiley Analytical Science Virtual Conference will bring together thousands of researchers and practitioners to share current developments in science and industry. Join for exciting presentations from experts in the fields of analytical and bioanalytical chemistry, pharmaceutical research, materials science, lab automation, and related disciplines.

Register to learn about recent developments & applications in:

- Microscopy
- Spectroscopy
- Mass Spectrometry
- Separation Science
- Much more!

**Register here**

**WILEY**

# Layered Transition Metal Oxides as Ca Intercalation Cathodes: A Systematic First-Principles Evaluation

Haesun Park,\* Christopher J. Bartel, Gerbrand Ceder, and Peter Zapol\*

**Finding high-voltage Ca cathode materials is a critical step to unleashing the full potential of high-energy-density Ca-ion batteries. First-principles calculations are used to demonstrate that P-type layered calcium transition metal (TM) oxide materials ( $\text{CaTM}_2\text{O}_4$ ) with a range of TM substitutions (TM = Ti, V, Cr, Mn, Fe, Co, and Ni) have excellent battery-related properties including thermodynamic stability, average voltage, energy density, synthesizability, ionic mobility, and electronic structure. However, the thermodynamic stability of the charged phase and TM redox activity are shown to be sensitive to TM selection, with  $\text{CaCo}_2\text{O}_4$  having the best balance of all considered properties. The utility of combining multiple TMs to expand the chemical search space for TM substitutions is demonstrated by mixing Co and Ni in layered  $\text{CaTM}_2\text{O}_4$ .**

## 1. Introduction

Energy storage devices that shuttle multivalent ions have attracted widespread attention as promising candidates for beyond Li-ion chemistry, due to their potential to meet the future needs of high voltage batteries at a reduced cost.<sup>[1]</sup> Among the multivalent chemistries being considered, systems with Ca metal anodes are particularly interesting due to the possibility of their voltage being higher than systems with Mg metal anodes. The standard electrode potential of Ca is lower than Mg by 650 meV, suggesting both higher voltage and superior energy density for Ca metal chemistry compared to Mg metal chemistry.<sup>[2]</sup> The abundant reserves of Ca are comparable

to Mg, and they are much higher than Li (Ca: 4.2%, Mg: 2.3%, Li: 0.002% of Earth's crust), suggesting low materials cost and a secure supply chain. Despite the inherent advantages of Ca-based chemistry, much less research efforts have been put in Ca than in Mg-based chemistries.

The emergence of Ca batteries has been hampered by the paucity of known materials functioning as electrolytes and electrodes. Recent development of electrolytes enabling facile Ca plating/stripping<sup>[3]</sup> and fast Ca intercalation into graphite<sup>[4]</sup> sparked renewed interest in Ca-based energy storage. Recent studies found that such classes of materials as


polyanionic phosphates,<sup>[5]</sup> Prussian Blue analogs,<sup>[6]</sup> and layered metal oxides<sup>[7,8]</sup> can reversibly accommodate Ca ions in non-aqueous systems; however, unlike for Mg, the design space for Ca cathode materials is still limited.

In Mg ion chemistry, high-throughput computational studies discovered that the ability to modify spinel compounds by transition metal (TM) substitution results in promising Mg intercalation hosts with high voltage, energy density, and fast cation diffusion in both oxides<sup>[9]</sup> and sulfides.<sup>[10]</sup> Following these computational screening efforts, experiments demonstrated the promise of oxide spinels as cathode hosts allowing reversible Mg intercalation,<sup>[11–13]</sup> and ternary spinel chalcogenides even attracted interest as Mg solid electrolytes.<sup>[14]</sup> Also, the high compositional flexibility of spinel in forming TM solid solutions opens up a broader space for searching Mg cathodes.<sup>[12]</sup> However, the absence of such theory-based guidelines for Ca cathodes has hindered the development of Ca-ion batteries.

Among the widely used structure types for conventional Li ion cathode materials (e.g., polyanion, layered, spinel), layered compounds with the nominal composition of  $\text{CaTM}_2\text{O}_4$  could be viable Ca cathode frameworks similar to spinel in Mg ion chemistry. Cabello et al. has shown that the P-type layered  $\text{CaCo}_2\text{O}_4$ , in which Ca cations are prismatically coordinated, can reversibly intercalate 0.35 mol of Ca and showed a capacity of 100 mAh  $\text{g}^{-1}$ .<sup>[7]</sup> Cushing et al. synthesized the two-layered (P2) or three-layered (P3)  $\text{Ca}_x\text{Co}_2\text{O}_4$  at Ca concentrations  $x$  including 0.52, 0.54, 0.70, and 1,<sup>[15]</sup> indicating that partially Ca deintercalated  $\text{CaCo}_2\text{O}_4$  is not susceptible to chemical decomposition and maintains the original host framework. The phase diagram calculated by density functional theory (DFT) also confirmed that the partially deintercalated  $\text{Ca}_x\text{Co}_2\text{O}_4$  ( $x = 0.5, 0.667, 0.7$ ) compounds are stable. Beside the thermodynamic stability, Ca diffusivity in P3- $\text{CaCo}_2\text{O}_4$  calculated by DFT using single ionic motion can be as low as 0.36 and 0.27 eV at the dilute and high

H. Park, P. Zapol  
Materials Science Division  
Joint Center for Energy Storage Research  
Argonne National Laboratory  
Lemont, IL 60439, USA  
E-mail: parkh@cau.ac.kr; zapol@anl.gov

H. Park  
School of Integrative Engineering  
Chung-Ang University  
Seoul 06974, Republic of Korea  
C. J. Bartel, G. Ceder  
Department of Materials Science and Engineering  
University of California  
Berkeley, CA 94720, USA  
G. Ceder  
Materials Science Division  
Lawrence Berkeley National Laboratory  
Berkeley, CA 94720, USA

 The ORCID identification number(s) for the author(s) of this article can be found under <https://doi.org/10.1002/aenm.202101698>.

DOI: 10.1002/aenm.202101698

vacancy concentration limits, respectively.<sup>[16]</sup> Moreover, Ca diffusivity for the partially deintercalated compound  $\text{Ca}_{0.5}\text{Co}_2\text{O}_4$  evaluated by stochastic sampling of Ca hopping was comparable to Li diffusivity in a conventional Li cathode.<sup>[16]</sup> Also, given that the various structures and compositions of layered  $\text{TM}_2\text{O}_4$  are also used for intercalating the ions whose ionic radii (e.g., Na: 116 pm K: 152 pm) are larger than Ca (114 pm), we can expect that the Ca ion can also reversibly intercalate into layered TM oxides.

In this context, charting thermodynamic, chemical, electronic and transport properties of a range of layered  $\text{CaTM}_2\text{O}_4$  materials will accelerate the discovery of viable Ca intercalation cathodes by guiding experimental efforts to more promising candidates. The TM ions studied in this work include Ti, V, Cr, Mn, Fe, Co, and Ni. By substituting the TM ions in layered  $P1$ -,  $P2_1/m$ -,  $Pmmn$ -, and  $P2/m$ - $\text{CaTM}_2\text{O}_4$ , 28 cathode structures were generated and their thermodynamic stability, average intercalation voltage, energy density, conversion voltages, synthesizability, cation mobility, and electronic structure were assessed with DFT calculations.

The results show that P-type structures of layered  $\text{CaTM}_2\text{O}_4$  with various TMs show many desirable battery-related properties. However, phase stability in the charged state and TM versus O redox preference are sensitive to the TM selection. Therefore, alloying different TMs is proposed as a strategy for layered  $\text{CaTM}_2\text{O}_4$  cathode development and demonstrated through the analysis of  $\text{CaCoNiO}_4$ .

## 2. Results

### 2.1. Structures of Layered $\text{TM}_2\text{O}_4$

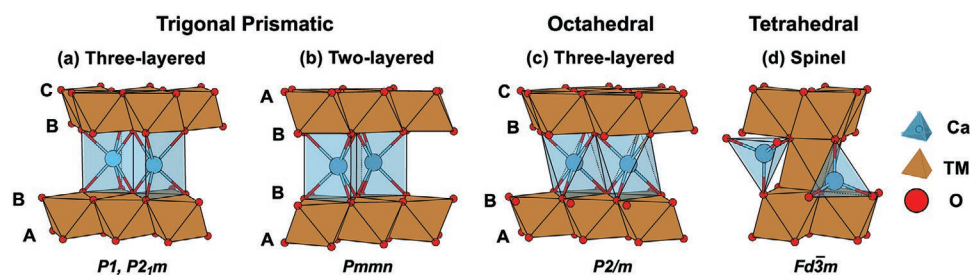
The structural motifs of layered compounds considered in this study are illustrated in **Figure 1**. The P-type layered structures with three (P3) and two (P2) oxygen stacking sequences with prismatically coordinated Ca ions are illustrated in Figure 1a,b, respectively. The  $\text{CaCo}_2\text{O}_4$  compounds with space group of  $P1$  and  $P2_1/m$  belong to the P3-layered structure.<sup>[15,17]</sup>  $\text{CaCr}_2\text{O}_4$  is another experimentally realized  $\text{CaTM}_2\text{O}_4$  having a space group of  $Pmmn$  and a P2-layered structure.<sup>[18]</sup> To fully explore the space of layered compounds, we also considered the O3-layered (space group  $P2/m$ ) structure, which is the ground-state structure for  $\text{Li}_{0.5}\text{CoO}_2$ , in which the alkali ions are octahedrally coordinated within a three-oxygen stacking sequence as depicted in

Figure 1c.<sup>[19]</sup> Finally, the spinel structure (space group:  $Fd\bar{3}m$ ) shown in Figure 1d was also studied to complement the evaluation of plausible  $\text{CaTM}_2\text{O}_4$  structures. In the spinel structure, Ca ions are tetrahedrally coordinated.

### 2.2. Thermodynamic Stability of Layered $\text{CaTM}_2\text{O}_4$

The thermodynamic stability of each  $\text{CaTM}_2\text{O}_4$  in each structure type was examined by calculating the energy above hull ( $E^{\text{hull}}$ ), which is the difference in energy of a given structure from the formation energy convex hull of ground states as a function of composition in the relevant Ca–TM–O phase diagram. If  $E^{\text{hull}} = 0$ , a compound is calculated to be stable with respect to decomposition into competing phases.  $E^{\text{hull}}$  values  $>0$  indicate possible metastable compounds, where compounds with small  $E^{\text{hull}}$  are often synthesizable<sup>[20]</sup> or accessible during electrochemical cycling. The  $E^{\text{hull}}$  of each TM substituted  $\text{CaTM}_2\text{O}_4$  (discharged state) and  $\text{TM}_2\text{O}_4$  (charged state) for the five different structure types are plotted in **Figure 2a** as a heatmap. In general, the P-type layered structures are more stable than O<sub>3</sub> and spinel compounds. According to Pauling's rule, Ca prefers a coordination number (CN) equal or greater than six when bonded with oxygen, stabilizing the P-type layered structure over the spinel. Although the CN of Ca in the O<sub>3</sub> structure is also six, the calculated energetics suggest that Ca prefers trigonal-prismatic coordination over octahedral environment in the layered structure.

Within P-type structures, compounds with Cr, Co, and Ni having a three-oxygen stacking sequence are fairly stable with  $E^{\text{hull}} < 7$  meV per atom as denoted by magenta circles in Figure 1a. The P-type  $\text{CaCr}_2\text{O}_4$  and  $\text{CaCo}_2\text{O}_4$  have been synthesized previously,<sup>[15,18]</sup> while layered  $\text{CaNi}_2\text{O}_4$  is newly reported in this work as potentially synthesizable, having comparable  $E^{\text{hull}}$  to these known materials. The Ti, V, Mn, and Fe substituted structures still have  $E^{\text{hull}}$  within 34 meV per atom, which falls within the typical hull energy range of experimentally known metastable oxides.<sup>[20]</sup> While nonlayered structures of  $\text{CaTi}_2\text{O}_4$ ,  $\text{CaMn}_2\text{O}_4$ , and  $\text{CaFe}_2\text{O}_4$  have been reported previously, the degree of metastability of layered compounds ( $E^{\text{hull}} < 34$  meV per atom) is comparable to many metastable compounds that have been synthesized.<sup>[20]</sup> In fact, polymorphs of many oxides having  $E^{\text{hull}} > 34$  meV per atom were reported to be synthesized, where the metastable polymorph can be stabilized without transforming into the ground state structure



**Figure 1.** The candidate crystal structures of nominal composition of  $\text{CaTM}_2\text{O}_4$ . The layered structure where the Ca atoms are prismatically coordinated in the two- and three-oxygen stacking structures are illustrated in a,b), respectively. The layered structure where the Ca atoms are octahedrally coordinated in the three-oxygen stacking structure is drawn in (c). The spinel structure is given at (d). The blue polyhedral, brown polyhedral, and red sphere represent the Ca, TM, and O, respectively. The space groups of the structures are given at the bottom.

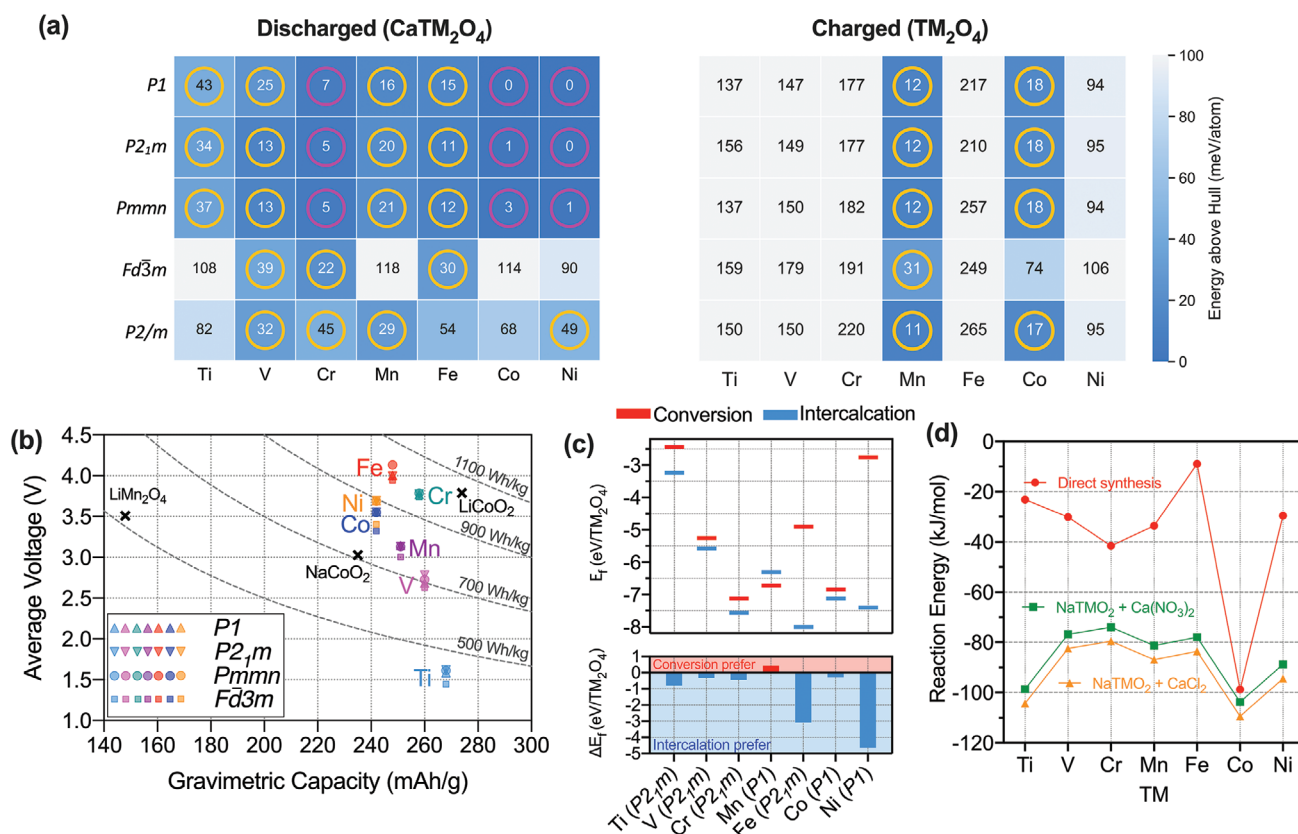


**Figure 2.** a) Energy above the convex hull ( $E^{\text{hull}}$ ) of various layered type  $\text{CaTM}_2\text{O}_4$  and  $\text{TM}_2\text{O}_4$ . The color and the annotation of each square in the heatmap represents  $E^{\text{hull}}$  of layered  $\text{CaTM}_2\text{O}_4$  or  $\text{TM}_2\text{O}_4$ , where the type of layer and the TM specie correspond to the ordinate and the abscissa, respectively. The magenta and yellow circles on the heatmap indicate the compound with  $E^{\text{hull}}$  within 10 meV per atom and 50 meV per atom, respectively. b) The computed average voltage versus gravimetric capacity for intercalation of Ca in various layered type of  $\text{TMO}_2$ . The color and the marker shape of data point convey the information of redox specie and the structure type, respectively. c) The preference between intercalation and conversion reaction upon Ca insertion into layered  $\text{TMO}_2$ . The horizontal blue and red lines represent the free energy of intercalation and conversion reaction, respectively. The free energy difference between two reactions is shown at the bottom, where positive value (blue area) and the negative value (red area) signify the preferential intercalation and conversion reaction, respectively. d) Formation energy for producing  $\text{CaTM}_2\text{O}_4$  by mean of ionic exchange between  $\text{NaTMO}_2$  and  $\text{CaCl}_2$  or  $\text{Ca}(\text{NO}_3)_2$ . The formation energies of  $\text{CaTM}_2\text{O}_4$  from binaries mixing is also plotted.

(e.g.,  $\text{CaCo}_2\text{O}_4$ ,  $\text{MgCr}_2\text{O}_4$ ).<sup>[7,13,21,22]</sup> This suggests that the metastable layered structures are potentially synthesizable and worth experimental efforts.

Among the fully charged states with all Ca ions extracted, layered  $\text{Mn}_2\text{O}_4$  and  $\text{Co}_2\text{O}_4$  are the most stable compounds. In the case of  $\text{MnO}_2$ , one may be concerned that partially deintercalated layered  $\text{Ca}_x\text{Mn}_2\text{O}_4$  transforms into the spinel phase because layered  $\text{LiMnO}_2$  instantly transforms into the spinel phase upon electrochemical cycling.<sup>[23]</sup> However, the layered phase of  $\text{NaMnO}_2$  does not undergo the phase transformation (to spinel) upon cycling because of the larger ionic size of Na compared to Li.<sup>[24]</sup> The layered  $\text{LiMnO}_2$  transforms to spinel during the Li deintercalation reaction due to the migration of Li to the tetrahedral site and subsequent migration of Mn to tetrahedral site, while, during the Na deintercalation from layered  $\text{NaMnO}_2$ , Na is unlikely to migrate to the tetrahedral site because of its large ionic size, thereby allowing for stable cycling without transformation.<sup>[24]</sup> Considering that the ionic radii of  $\text{Ca}^{2+}$  and  $\text{Na}^+$  are extremely similar, it is plausible for layered  $\text{Ca}_x\text{Mn}_2\text{O}_4$  to similarly remain layered upon deintercalation. The charged versions of all other TM layered structures

are much more metastable with  $E^{\text{hull}} > 90$  meV per atom. This indicates that upon full Ca deintercalation, these materials are susceptible to decomposition to alternative structures or compounds. The instability of the charged state will be discussed later in detail.

### 2.3. Electrochemical Characteristics of Intercalation Reactions

The average voltage of the intercalation reaction ( $\text{Ca} + \text{TM}_2\text{O}_4 \rightarrow \text{CaTM}_2\text{O}_4$ ) as a function of gravimetric capacity is given in Figure 2b where the shape and color of data points indicate structure types and redox species, respectively. The average voltages are referenced to fcc Ca metal. The average voltages of Li and Na compounds are obtained from Materials Project<sup>[25]</sup> where the values are obtained using the same level of theory as our calculations. Clearly, the layered compounds exhibit larger average intercalation voltages than spinel by at most 0.29 V. However, as depicted in Figure 2a, the average voltages are more clustered according to the TM species than the structure type, indicating strong sensitivity of the average voltage to redox

species. The compounds with TM species of V, Cr, Mn, Fe, Co, and Ni, exhibit average voltages greater than 2.7 V, whereas the Ti-containing compound yields relatively low voltage ( $\approx 1.5$  V), which is more suitable for anodes (e.g.,  $\text{Li}_4\text{Ti}_5\text{O}_{12}$ ).<sup>[26]</sup>

Generally, the average voltages of layered  $\text{CaTM}_2\text{O}_4$  are lower than those of spinel- $\text{LiMn}_2\text{O}_4$  (3.51 V vs  $\text{Li}/\text{Li}^+$ , layered  $\text{CaMn}_2\text{O}_4$ : 3.15 V vs  $\text{Ca}/\text{Ca}^{2+}$ ) and layered  $\text{LiCoO}_2$  (3.79 V vs  $\text{Li}/\text{Li}^+$ ; layered  $\text{CaCo}_2\text{O}_4$ : 3.56 V vs  $\text{Ca}/\text{Ca}^{2+}$ ), but the voltage penalty compared to the Li analogs is less than 0.36 V. However, the divalency of Ca allows superior gravimetric capacity and specific energy over lithium spinel. Even when the layered  $\text{CaTM}_2\text{O}_4$  compounds are compared with  $\text{LiCoO}_2$  and  $\text{NaCoO}_2$ , which also utilize  $\text{TM}^{3+}/\text{TM}^{4+}$  redox, the theoretical gravimetric capacity is comparable to  $\text{LiCoO}_2$  (274  $\text{mAh g}^{-1}$ ,  $\text{CaCo}_2\text{O}_4$ : 242  $\text{mAh g}^{-1}$ ) and even outperforms  $\text{NaCoO}_2$  (235  $\text{mAh g}^{-1}$ ). Similarly, the volumetric capacity and energy density of layered  $\text{CaTM}_2\text{O}_4$  is comparable to those of layered  $\text{LiCoO}_2$  and outperformed the layered  $\text{NaCoO}_2$  (Figure S2, Supporting Information). In light of these calculated energy densities, the layered  $\text{CaTM}_2\text{O}_4$  compounds are intriguing Ca intercalation cathodes.

A possible performance-limiting phenomenon that can occur during battery operation, in particular during the discharge, is undesired chemical conversion (e.g., decomposition to alternative phases) during electrochemical insertion of Ca ions, which can result in irreversible capacity loss. The thermodynamic preference between intercalation and conversion reactions can be gauged by comparing the energy of each reaction.<sup>[27]</sup> The considered conversion reactions upon Ca insertion into various layered  $\text{TM}_2\text{O}_4$  are summarized in Note S1 in the Supporting Information. The energies for intercalation ( $\text{Ca} + \text{TM}_2\text{O}_4 \rightarrow \text{CaTM}_2\text{O}_4$ ) and conversion reactions are plotted in Figure 2(c), with the differences between the two energies plotted at the bottom. The analysis reveals that the energy for the intercalation reaction is lower than for conversion for all TM species except Mn. The reaction reducing Mn from +4 to +3 by topotactic Ca ion insertion is thermodynamically unfavorable and Mn prefers to disproportionate to +2.67 ( $\text{Mn}_3\text{O}_4$ ) and +4 ( $\text{Ca}_2\text{Mn}_3\text{O}_8$ ) compounds, unless slow kinetics limits this conversion reaction. Except for the layered  $\text{Mn}_2\text{O}_4$ , the layered compounds prefer the intercalation reaction and show conversion resistance, further supporting these layered compounds as viable Ca intercalation cathodes.

Although some discharged materials are calculated to be thermodynamically stable, kinetic and/or thermodynamic constraints possibly hinder the synthesis of phase-pure compounds. The representative example of such constraints in multivalent cathodes is the spinel  $\text{MgCr}_2\text{S}_4$ .<sup>[28]</sup> DFT calculations predicted  $\text{MgCr}_2\text{S}_4$  to be thermodynamically stable, but the calculated reaction energy for its formation from  $\text{MgS} + \text{Cr}_2\text{S}_3$  is very small (2  $\text{kJ mol}^{-1}$ ). This manifests in solid-state synthesis from the binary sulfide precursors requiring high firing temperature and long holding times (800 °C for two weeks).<sup>[29]</sup> Miura et al. showed that the ion-exchange metathesis reaction ( $\text{MgCl}_2 + 2\text{NaCrS}_2 \rightarrow \text{MgCr}_2\text{S}_4 + 2\text{NaCl}$ ) has a larger reaction energy of -47  $\text{kJ mol}^{-1}$ , which greatly sped up the synthesis (500 °C for 30 minutes).<sup>[28]</sup> A similar metathesis was also demonstrated in the synthesis of layered  $\text{Ca}_x\text{Co}_2\text{O}_4$  from  $\text{Na}_{2x}\text{Co}_2\text{O}_4 + x\text{Ca}(\text{NO}_3)_2$ .<sup>[15]</sup>

The utility of metathesis synthesis for each candidate  $\text{CaTM}_2\text{O}_4$  was evaluated by comparing the reaction energies for ion exchange (layered  $\text{NaTMO}_2 + \text{CaCl}_2$  or  $\text{Ca}(\text{NO}_3)_2$ ) and solid-state synthesis as plotted in Figure 2d. The reactions for solid-state synthesis from the commercially available oxide precursors are listed in Note S2 in the Supporting Information. The reaction energies to form layered  $\text{CaTM}_2\text{O}_4$  by ion exchange from layered  $\text{NaTMO}_2$  are approximately twice larger than those by solid-state synthesis. This shows that metathesis has a larger thermodynamic driving force than solid-state reactions for every TM evaluated. In the case of  $\text{CaCo}_2\text{O}_4$ , energies for the solid-state reaction and the ion exchange are similar ( $\approx 100$   $\text{kJ mol}^{-1}$ ), but still the route through the ion exchange exhibits slightly larger reaction energy. Although the difference is marginal, the reaction through ion exchange using  $\text{CaCl}_2$  salt is thermodynamically more favorable than using  $\text{Ca}(\text{NO}_3)_2$  salt in all cases. The formation of layered  $\text{CaTM}_2\text{O}_4$  through the ion exchange from the layered  $\text{LiTMO}_2$  (instead of  $\text{NaTMO}_2$ ) are endothermic reactions (Figure S1, Supporting Information). The ion-exchange reactions with Na to make layered  $\text{CaTM}_2\text{O}_4$  have higher driving force than the reactions with Li because the ion-exchange reaction with the respective chlorides/nitrates to make  $\text{LiTMO}_2$  from  $\text{NaTMO}_2$  is exothermic.

#### 2.4. Ca Ion Migration Barriers in Layered Frameworks

Cathode materials should have facile diffusion for the working cations to enable the topotactic intercalation reactions. However, this requirement is expected to be more difficult to achieve for Ca than for Li because the divalent Ca ion will interact more strongly with oxygen in the material. Interestingly, our previous study showed that the Ca migration barrier in P3-type layered  $\text{CaCo}_2\text{O}_4$  can be as low as 0.36 and 0.27 eV at the dilute ( $\text{Ca}_{0.9375}\text{TM}_2\text{O}_4$ ) and high ( $\text{Ca}_{0.0625}\text{TM}_2\text{O}_4$ ) vacancy concentration limits, respectively.<sup>[16]</sup> Hence, we evaluated whether the low Ca migration barrier characteristic of layered structures still holds upon TM substitution.

Figure 3a depicts the energies for Ca ion migration at the dilute vacancy limit ( $\text{Ca}_{0.9375}\text{TM}_2\text{O}_4$ ) in the P3-type layered structures (P1 and  $\text{P}_{21/m}$ ). The migration barriers, which are the difference between the minimum and maximum of DFT-calculated minimum energy pathways, are charted in Table S2 in the Supporting Information. In general, in both P1 and  $\text{P}_{21/m}$ , the Ca ion migration barriers range from 0.28 to 0.47 eV for all TM species except P1- $\text{CaMn}_2\text{O}_4$  (0.81 eV). The deviation in migration energy for P1- $\text{CaMn}_2\text{O}_4$  originates from the large structural difference with other P1  $\text{CaTM}_2\text{O}_4$  structures due to the  $\text{Mn}^{3+}$  Jahn–Teller distortion (Figure S3, Supporting Information). Although a Jahn–Teller distortion is observed in  $\text{P}_{21/m}$ - $\text{CaMn}_2\text{O}_4$  as well, the overall structural distortion is marginal (Figure S4, Supporting Information), and the Ca migration barrier shows a similar trend with  $\text{P}_{21/m}$  structures containing other TMs.

In P2-type  $\text{Pmmn}$  structures, Ca ion migration barriers are a bit higher than P1 and  $\text{P}_{21/m}$  structures as shown in Figure 3b. Although migration barriers surge to 1.15 eV in  $\text{Pmmn-CaMn}_2\text{O}_4$  at the extreme, in general, the migration barriers are between 0.53 and 0.71 eV. The higher Ca migration

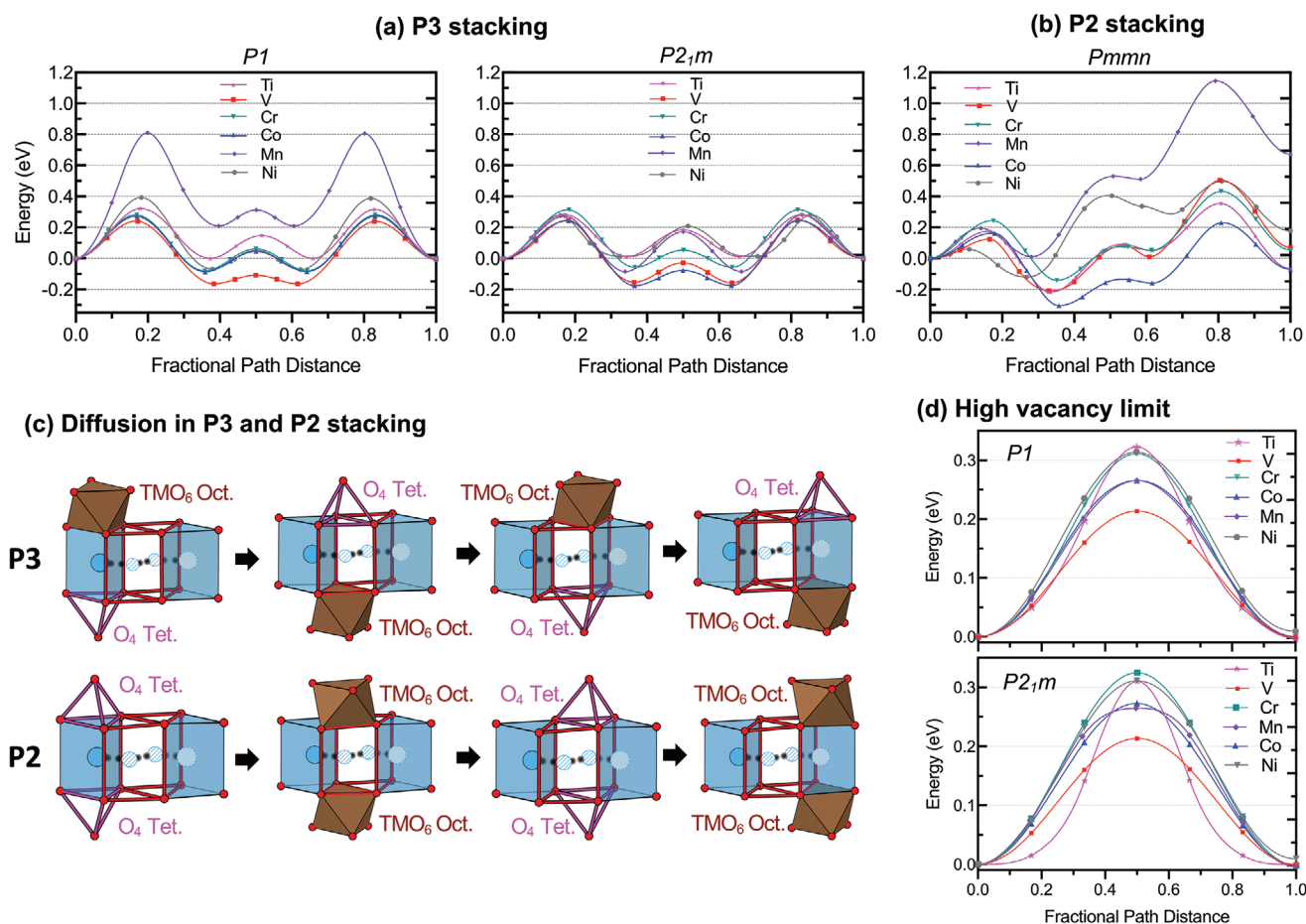


**Figure 3.** The minimum energy pathways for migration of Ca ion at the dilute vacancy limit in the various TM substituted layered  $\text{CaTM}_2\text{O}_4$  with a) P3 stacking (space group: P1, P<sub>21</sub>/m) and b) P2 stacking (space group: Pmmn). c) Environments for Ca hopping in the layered  $\text{CaTM}_2\text{O}_4$  with P3 and P2 stackings. Blue and red triangular prisms represent initial/final states and intermediate transition states, respectively. Brown octahedron (oct.) and magenta tetrahedron (tet.) illustrate TM and O<sub>4</sub> environments of the ends of triangular prisms, respectively. The Ca migration barriers at the high vacancy limit in P3 stacking structures are given in (d).

barrier in P2-type than P3-type structures can be explained in terms of the environments encountered by the diffusing Ca. The energy for cation migration is partly dictated by the coordination environment of the diffusing Ca ion at the transition states. In both P2- and P3-type structures, the Ca ion migrates through the two triangular prisms as shown in Figure 3c; however, the local environments in each prism are not the same. In the P3-type structure, each prism shares its top and bottom face with a TMO<sub>6</sub> octahedron or an O<sub>4</sub> tetrahedron, respectively, along the entire migration pathway. This consistency of local environment during diffusion results in a relatively flat energy landscape and low migration barriers. However, in the P2-type structure, the prism at the initial state shares its top and bottom sides with an O<sub>4</sub> tetrahedron, while the next prism, which is the first transition state shares top and bottom with TMO<sub>6</sub> octahedron. The next prism, which contains the second transition state, shares a face with an O<sub>4</sub> tetrahedron again and the final state does the same with a TMO<sub>6</sub> octahedron. Such stronger fluctuations of coordination environment in P2-type compared to P3-type result in larger energy variations along the diffusion path, increasing migration barriers.

The energy profile along the Ca ion migration path at the high vacancy limit ( $\text{Ca}_{0.0625}\text{TM}_2\text{O}_4$ ) in P3-type layered structures is shown in Figure 3(d). The activation energies are less than 0.33 eV, which is quite low, suggesting the facile insertion of Ca into bulk  $\text{TM}_2\text{O}_4$  at the onset of discharge for the entire range of TMs studied, at least from a kinetic perspective. When compared with migration barriers of Li in layered  $\text{CoO}_2$  (between  $\approx 0.2$  and  $\approx 0.6$  eV via a divacancy mechanism),<sup>[30]</sup> the calculated Ca mobility in the layered  $\text{TMO}_2$  is deemed to be sufficient for cathode materials. Although not suitable for high rate application, migration barriers below 0.65 eV are satisfactory for cathode materials in practical charging and discharging conditions for cathode particles below 100 nm,<sup>[9]</sup> indicating the Ca-ion migration barriers calculated from this study are acceptable.

## 2.5. TM Redox Activity from Electronic Structure

The strategy to design layered  $\text{CaTM}_2\text{O}_4$  as a cathode material is to utilize TM species as redox centers that maintain the electro-neutrality during (de)intercalation of working cations. However,

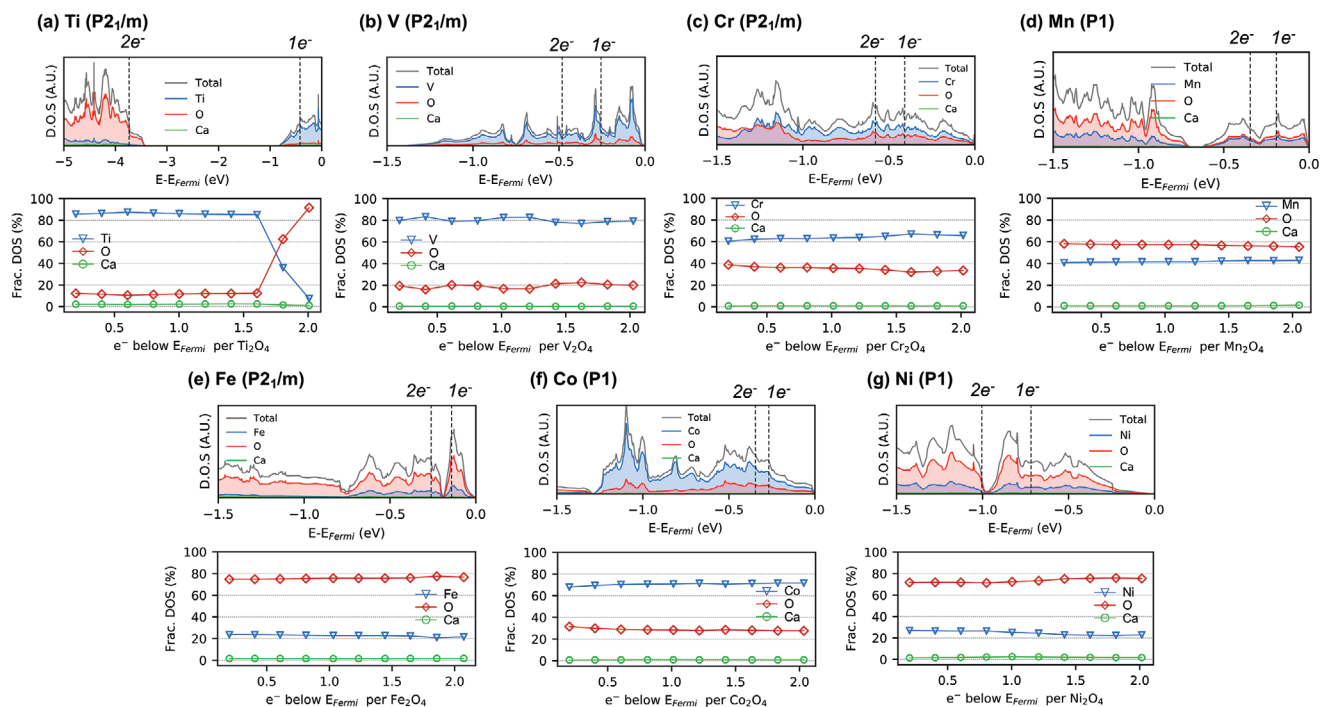


**Figure 4.** Atom-PDOS and the contribution of each species to total DOS of the various TM: a) Ti, b) V, c) Cr, d) Mn, e) Fe, f) Co, g) Ni substituted  $\text{CaTM}_2\text{O}_4$ . In the PDOS plot, the grey, blue, red, and green represent the total DOS, TM PDOS, O PDOS, and Ca PDOS, respectively. The DOS is in an arbitrary unit (AU). The dashed lines indicate the energy levels where the total number of electrons from Fermi energy are one and two, respectively. The contribution of PDOS to the total DOS was sampled approximately every  $0.2e^-$  and the fraction of each species in total DOS is plotted below the PDOS plot.

in some layered cathode materials, O redox contributes to charge compensation.<sup>[31]</sup> Under the assumption that redox phenomena are related to the nature of electronic states participating in redox, we attempt to predict the redox mechanism by scrutinizing the electronic structure of the discharged materials.

**Figure 4** shows the atom-projected density of states (PDOS) of each species (Ca, TM, and O) in the layered  $\text{CaTM}_2\text{O}_4$  and their fraction of the total density of states (DOS). When a Ca ion is removed from the structure, electrons in the highest occupied states at or below the Fermi energy are likely to be oxidized. Building upon classic work understanding redox couples in Li-ion batteries,<sup>[32]</sup> we posit that for TM redox to dominate upon initial oxidation (Ca removal), the electron density near the Fermi energy should be dominated by the TM and weakly coupled to O.<sup>[33]</sup> We are particularly interested in the character of the  $2e^-$  closest to the Fermi energy as these are the  $e^-$  that must be oxidized to accommodate the removal of 1 Ca per  $\text{CaTM}_2\text{O}_4$ . In the Ti and V compounds (Figure 4a,b), the TM states comprise more than 80% of the total DOS immediately below the Fermi energy with relatively small coupling to O states, implying preferential electron extraction from the TM (TM oxidation) upon deintercalation. However, the TM PDOS in  $\text{CaTi}_2\text{O}_4$  no longer dominates the total DOS  $\approx 3.5$  eV below the Fermi energy as the O states make up the largest part of the total DOS at these energies. The total number of electrons occupying states from the Fermi energy to this level is  $\approx 1.5e^-$ , which corresponds to the extraction of  $0.75 \text{ Ca}^{2+}$  per  $\text{CaTi}_2\text{O}_4$  via Ti redox. For Cr and Co compounds (Figure 4c,f), the TM PDOS comprises 60% and 70% of total DOS over the range of  $2e^-$  removal, respectively,

suggesting some coupling of the TM d with O p states, but the TM remains the dominant component of the DOS.

For Mn, Fe, and Ni compounds (Figure 4d,e,g), the O states account for more than 60% of total DOS near the Fermi energy suggesting a higher degree of hybridization of TM and O states than for other compounds. Under the assumption of rigid density of states and local bonding character upon Ca removal, electrons are likely to be extracted from oxygen, resulting in TM oxidation through charge transfer or oxygen oxidation in the form of peroxy-like  $\text{O}_2^{2-}$  formation. While the latter could entail oxygen evolution reactions that lead to irreversible structural transformation or electrolyte decomposition, the validity of the assumptions made needs to be further tested. This method of analyzing the electronic structure of the fully discharged materials provides an initial and high-throughput evaluation of the potential redox behavior upon Ca extraction but is not a comprehensive means by which to assess the plausibility of reversible redox upon (de-)intercalation.

### 3. Discussion

In this study, we evaluated the electrochemical, thermodynamic, kinetic, and electronic properties of Ca ion intercalation in layered TM oxides by means of first-principles calculations. A summary of battery-related properties of layered  $\text{CaTM}_2\text{O}_4$  is presented in **Figure 5a** as a radar plot. The migration barriers are obtained by averaging the values at the dilute and high vacancy limits.

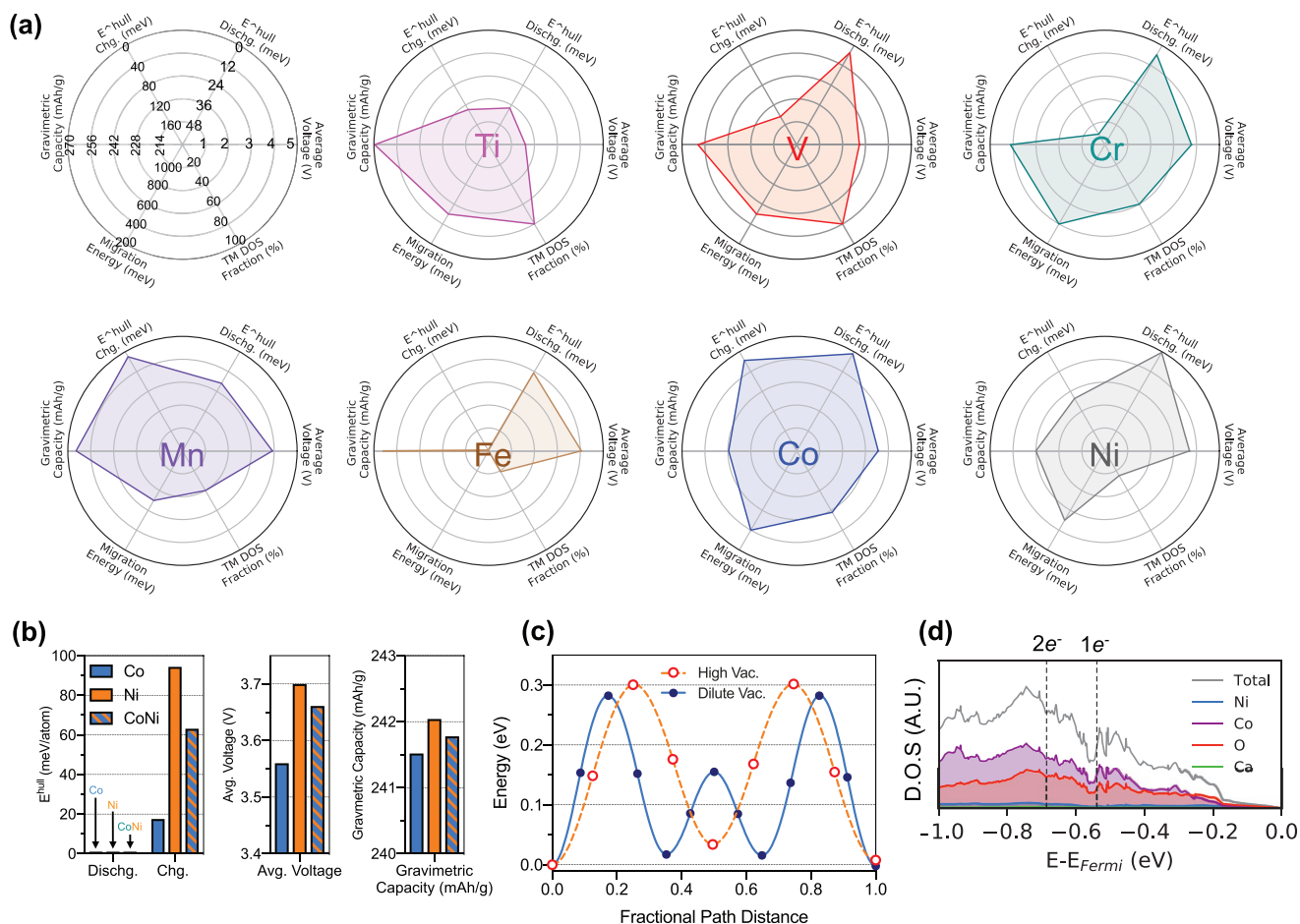


**Figure 5.** a) Radar plots of the calculated battery-related properties of layered  $\text{CaTM}_2\text{O}_4$ . b) Energy above hull, average intercalation voltage, and gravimetric capacity of layered  $\text{CaCoNiO}_4$ ,  $\text{CaCo}_2\text{O}_4$ , and  $\text{CaNi}_2\text{O}_4$  compounds. c) The minimum energy pathways for Ca migration in the layered  $\text{CaCoNiO}_4$  at dilute vacancy limit. d) Partial density of states plot of layered  $\text{CaCoNiO}_4$  compound.

In general, layered  $\text{CaTM}_2\text{O}_4$  compounds show excellent thermodynamic stability of the discharged phase, low cation migration barrier, high average cell voltage, and high energy density, but the stability of the charged phase and the apparent preference for TM versus O redox are sensitive to the TM selection. For example, the compounds with Ti, V, and Cr are predicted to undergo TM redox upon intercalation because of the larger TM PDOS fraction (compared to O) just below the Fermi energy. However, their charged phases exhibit high  $E^{\text{hull}}$  because of the instability of the charged layered phase with respect to the rutile structure, suggesting the potential for phase change at high states of charge. In contrast, the Mn compound has a larger O than TM PDOS fraction just below the Fermi energy and a small  $E^{\text{hull}}$  at the charged phase. In the case of Ni and Fe compounds, the  $E^{\text{hull}}$  of the charged phase is large and the fraction of O PDOS is greater than TM PDOS near the Fermi energy. Only the Co compound exhibits a relatively high stability at the charged state and has a DOS near the Fermi energy dominated by TM states. Given the efforts to minimize the use of Co in battery cathode materials,<sup>[34]</sup> it is imperative to design materials with a smaller Co to Ca ratio than  $\text{CaCo}_2\text{O}_4$ .

One pathway toward this goal is to replace some fraction of Co with other TM species. This method is commonly used in the design of layered oxides for Li and Na cathodes.<sup>[35]</sup> One of the TM species that can partially substitute Co is Ni, which is chosen for higher average voltage and for the practical reason of relatively higher supply.<sup>[34,36]</sup> The charged phase of the pure Ni compound is very unstable ( $E^{\text{hull}} = 94$  meV per atom) and O redox at the initial charge is expected based on the results of our calculations on layered  $\text{CaNi}_2\text{O}_4$ . The hope is that by mixing Co and Ni, we can take advantage of the desirable stability and redox properties of  $\text{CaCo}_2\text{O}_4$  while diminishing the fraction of Co in the sample.

The analysis of phase stability, average cell voltage, and energy density for  $\text{CaCoNiO}_4$  is plotted in Figure 5b. The phase diagram analysis indicates that layered  $\text{CaCoNiO}_4$  (discharged) is thermodynamically stable ( $E^{\text{hull}} = 0$  meV per atom) with respect to the pure Co and Ni compounds. Interestingly, the charged phase ( $\text{CoNiO}_4$ ) exhibits  $E^{\text{hull}}$  of 61 meV per atom, which is between that of layered  $\text{Co}_2\text{O}_4$  (18 meV per atom) and  $\text{Ni}_2\text{O}_4$  (94 meV per atom). The partially decalcated state ( $\text{Ca}_x\text{CoNiO}_4$ ) can still be retained given that the Na analog ( $\text{Na}_2\text{CoNiO}_4$ ) has been shown to partially deintercalate sodium.<sup>[37]</sup> To confirm



the stability of the partially decalcated state, we calculated the  $E^{\text{hull}}$  of half-calcated  $\text{Ca}_{0.5}\text{CoNiO}_4$ , and it is only 19 meV per atom, suggesting the feasibility of cycling at least 0.5 mol Ca. The average voltage and gravimetric capacity of  $\text{CaCoNiO}_4$  (3.66 V, 241.8 mAh  $\text{g}^{-1}$ ) resides between the pure Ni (3.70 V, 242.0 mAh  $\text{g}^{-1}$ ) and Co (3.56 V, 241.5 mAh  $\text{g}^{-1}$ ) compounds.

The minimum energy pathways for Ca migration in layered  $\text{CaCoNiO}_4$  in the dilute and high vacancy limits are plotted in Figure 5c. Ca diffusion is calculated to be facile with migration barriers of 0.28 and 0.30 eV at the dilute and high vacancy limits, respectively. These are comparable to the migration barriers in the pure Co or Ni compounds, indicating that mixing two TM species does not significantly affect the Ca diffusion barrier. This confirms that the fast diffusion of Ca is not particularly sensitive to the selection of TM(s).

The electronic structure properties responsible for redox during intercalation in layered  $\text{CaCoNiO}_4$  were analyzed using the PDOS plot shown in Figure 5d. From the Fermi energy to the energy level equivalent to  $1e^-$  of integrated density of states (corresponding with 0.5  $\text{Ca}^{2+}$  extracted per  $\text{CoNiO}_4$ ), the PDOS of Co is larger than those of other species. This alleviates the strong O PDOS coupling near the Fermi energy in the layered  $\text{CaNi}_2\text{O}_4$ , suggesting TM redox activity upon initial Ca ion deintercalation in  $\text{CaCoNiO}_4$ . Interestingly, in the Na analog (layered  $\text{NaCo}_{0.5}\text{Ni}_{0.5}\text{O}_2$ ), an analysis of the calculated magnetic moments suggested that the oxidation of Ni precedes that of Co, contrary to our results for  $\text{CaCoNiO}_4$ .<sup>[37]</sup> To support Co oxidation upon Ca extraction, we compare the calculated magnetic moments of TM species of  $\text{CaCoNiO}_4$  and  $\text{Ca}_{0.5}\text{CoNiO}_4$ . The average magnetic moments of Co and Ni in  $\text{CaCoNiO}_4$  are  $-0.01$  and  $1.21 \mu_{\text{B}}$ , respectively, indicating the trivalency of both TM species. In  $\text{Ca}_{0.5}\text{CoNiO}_4$ , the magnetic moment of Co becomes  $1.06 \mu_{\text{B}}$ , which corresponds to the tetravalent Co ion, while that of Ni is unchanged, supporting that Co oxidation occurs prior to Ni oxidation, as suggested by the PDOS analysis.

Our calculations provide evidence that substituting some portion of Co with Ni can compensate the drawbacks of  $\text{CaNi}_2\text{O}_4$  by increasing the thermodynamic stability of the charged phase and the redox activity of TM ion. This strategy can effectively reduce the amount of Co in the cathode materials by increasing the utilization of Ni instead of Co. TM mixing is not just limited to Ni but could potentially incorporate many other species, including not only 3d TMs but also the 4d or 5d species, enlarging the design space for layered Ca cathode materials.

## 4. Conclusion

The absence of design guidelines for Ca intercalation cathodes has hampered the emergence of a battery utilizing Ca as a working cation. Here, we used DFT calculations to show that various TM-substituted layered oxides can be a new avenue for Ca cathodes. First-principles calculations were performed for  $\text{CaTM}_2\text{O}_4$  materials across seven different TM species (Ti, V, Cr, Mn, Fe, Co, and Ni) for four layered polymorphs ( $P1$ ,  $P2_1/m$ ,  $Pm\bar{m}n$ , and  $P2/m$ ) to assess their thermodynamic stability, average intercalation voltage, energy density, preference for intercalation versus conversion, synthesizability, cation mobility, and electronic structure.

The P-type layered discharged materials ( $P1$ ,  $P2_1/m$ ,  $Pm\bar{m}n$ ) are fairly stable and more stable than  $\text{O}_3$  ( $P2/m$ ) and spinel compounds, whereas the charged structures are less stable due to competition with alternative (nonlayered)  $\text{TM}_2\text{O}_4$  phases. The average voltages of layered  $\text{CaTM}_2\text{O}_4$  are lower than those in Li compounds but the voltage penalty is less than 0.36 V, while the multivalent Ca results in better gravimetric capacity. The Ca ion intercalation reaction is more favorable than conversion reactions for all TM species except  $\text{CaMn}_2\text{O}_4$ . Metathesis synthesis from  $\text{NaTMO}_2$  and  $\text{CaCl}_2/\text{Ca}(\text{NO}_3)_2$  has larger thermodynamic driving force than solid-state synthesis, suggesting a facile way to create the discharged materials.

The Ca ion migration barriers in the dilute vacancy limit for P3-type structures are quite small and generally similar for different TM substitutions, within the range of less than 0.33 eV. Upon Ca extraction, the redox mechanism is predicted to involve TM 3d states, except for Ni, Fe, and Mn, where the presence of substantial oxygen states near the Fermi energy may render them less promising cathode materials. However, forming a Co/Ni alloy,  $\text{CaCoNiO}_4$ , increases the Co 3d state near the Fermi level and enhances the thermodynamic stability of the fully charged state, compared to the Ni-only compound. At the same time,  $\text{CaCoNiO}_4$  has a higher voltage than the Co-only compound. This design strategy will be further exploited in screening different TM combinations to identify novel Ca cathode materials with improved properties. To further deepen our understanding of layered  $\text{CaTM}_2\text{O}_4$  as a cathode for CIB and enhance the performance of this system, investigating possible anionic redox reactions<sup>[38]</sup> and optimizing  $\text{CaTM}_2\text{O}_4$  by doping<sup>[39]</sup> would be promising future directions. Also, calculating vibrational properties and voltage behavior would be helpful to predict thermodynamic properties at finite temperatures and the electrochemical behavior of the system, respectively.<sup>[39]</sup>

In total, by comprehensively evaluating the thermodynamic, kinetic, and electronic properties of layered  $\text{CaTM}_2\text{O}_4$  materials relevant to synthesis and electrochemical cycling, we show that this class of materials may open up a tremendous design space for the future of cathode materials for Ca batteries.

## 5. Experimental Section

First-principles calculations were performed based on DFT<sup>[40]</sup> as implemented in the Vienna ab initio simulation package.<sup>[41]</sup> The core electron contributions were described by the projector-augmented wave<sup>[42]</sup> potentials and the valence electrons were described by the plane-wave basis set with a cutoff energy of 520 eV. The generalized gradient approximation form of the electron exchange-correlation functional by Perdew–Burke–Ernzerhof<sup>[43]</sup> was employed. The unphysical delocalization of d-electrons of the TM species was remedied with the addition of Hubbard U correction, and the U value of each TM species was taken from Wang et al.<sup>[44]</sup> A ferromagnetic configuration was set for the initial state of unpaired electrons. The k-points were generated by the Python Materials Genomics (pymatgen) code<sup>[45]</sup> with a density of 1500/reciprocal atom ( $5 \times 4 \times 4$  for  $P1$  and  $P2_1/m$ ,  $2 \times 3 \times 4$  for  $Pm\bar{m}n$ ,  $4 \times 4 \times 1$  for  $P2/m$ ,  $5 \times 5 \times 5$  for  $Fd\bar{3}m$ ). For PDOS plots, a denser k-point mesh was used for the more accurate calculations of electronic structures ( $9 \times 7 \times 7$  for  $P1$  and  $P2_1/m$ ,  $5 \times 9 \times 10$  for  $Pm\bar{m}n$ ). The  $P1$ ,  $P2_1/m$ , and  $P2/m$  structures were adopted from the set of  $\text{CaCo}_2\text{O}_4$  structures used in the previous studies.<sup>[16,22]</sup> The  $Pm\bar{m}n$  and  $Fd\bar{3}m$  structures were taken from the Inorganic Crystal Structure Database.<sup>[18,46]</sup>

The phase diagram of Ca–TM–O was calculated using relevant compounds obtained from the Materials Project<sup>[25]</sup> and all structures were fully relaxed to the atomic force tolerance of 0.02 eV Å<sup>-1</sup>. Then, the phase diagram was constructed using the pymatgen code to determine the  $E^{\text{hull}}$  of charged and discharged phases.<sup>[47]</sup> The average voltage ( $V_{\text{average}}$ ) for Ca intercalation between charged (TM<sub>2</sub>O<sub>4</sub>) and discharged (CaTM<sub>2</sub>O<sub>4</sub>) phase was calculated as

$$V_{\text{average}} = \frac{E_{\text{chg.}} + nE_{\text{Ca}} - E_{\text{dischg.}}}{nz} \quad (1)$$

where  $E_{\text{chg.}}$ ,  $E_{\text{dischg.}}$ , and  $E_{\text{Ca}}$  are the total energies of charged, discharged phases, and fcc Ca metal;  $n$  is the number of Ca ions associated with the intercalation reaction;  $z$  is the oxidation state of Ca ion (+2). Energy densities were evaluated on the basis of intercalating 1 mol Ca per TM<sub>2</sub>O<sub>4</sub> (equivalently 0.5 mol per TMO<sub>2</sub>).

The Ca migration barriers were calculated with the climbing image nudged elastic band (NEB)<sup>[48]</sup> method. The supercell approach ( $2 \times 2 \times 2$  for *P1* and *P2<sub>1</sub>/m*,  $2 \times 2 \times 1$  for *Pmmn*) was used to avoid fictitious interactions among the diffusing Ca atoms in the periodic images and the inter-image distance was set to be at least 9 Å. The NEB calculations were relaxed to the atomic force tolerance of 0.05 eV Å<sup>-1</sup>.

## Supporting Information

Supporting Information is available from the Wiley Online Library or from the author.

## Acknowledgements

This work was supported as part of the Joint Center for Energy Storage Research, an Energy Innovation Hub funded by the U.S. Department of Energy, Office of Science, Basic Energy Sciences. The work at Argonne National Laboratory (ANL) was performed under contract no. DE-AC02-06CH11357. This manuscript has been authored by employees of Lawrence Berkeley National Laboratory under Contract No. DE-AC02-05CH11231 with the U.S. Department of Energy. The U.S. Government retains, and the publisher, by accepting the article for publication, acknowledges, that the U.S. Government retains a non-exclusive, paid-up, irrevocable, world-wide license to publish or reproduce the published form of this manuscript, or allow others to do so, for U.S. Government purposes.

## Conflict of Interest

The authors declare no conflict of interest.

## Data Availability Statement

The data that support this study are available from the corresponding author upon reasonable request.

## Keywords

calcium-ion batteries, cathode materials, first-principles calculations, layered transition metal oxides, multivalent batteries

Received: May 31, 2021  
Revised: October 4, 2021  
Published online:

- [1] Y. Liang, H. Dong, D. Aurbach, Y. Yao, *Nat. Energy* **2020**, *5*, 646.
- [2] a) A. Ponrouch, M. R. Palacin, *Curr. Opin. Electrochem.* **2018**, *9*, 1; b) M. E. Arroyo-de Dompablo, A. Ponrouch, P. Johansson, M. R. Palacin, *Chem. Rev.* **2019**, *120*, 6331; c) P. Vanýsek, in *CRC Handbook of Chemistry and Physics*, (Ed: J. Rumble), CRC Press LLC, Boca Raton, FL **2019**.
- [3] a) D. Wang, X. Gao, Y. Chen, L. Jin, C. Kuss, P. G. Bruce, *Nat. Mater.* **2018**, *17*, 16; b) M. Wang, C. Jiang, S. Zhang, X. Song, Y. Tang, H.-M. Cheng, *Nat. Chem.* **2018**, *10*, 667; c) Z. Li, O. Fuhr, M. Fichtner, Z. Zhao-Karger, *Energy Environ. Sci.* **2019**, *12*, 3496; d) A. Shyamsunder, L. E. Blanc, A. Assoud, L. F. Nazar, *ACS Energy Lett.* **2019**, *4*, 2271; e) S. Biria, S. Pathreker, F. S. Genier, H. Li, I. D. Hosein, *ACS Appl. Energy Mater.* **2020**, *3*, 2310; f) S. D. Pu, C. Gong, X. Gao, Z. Ning, S. Yang, J.-J. Marie, B. Liu, R. A. House, G. O. Hartley, J. Luo, P. G. Bruce, A. W. Robertson, *ACS Energy Lett.* **2020**, *5*, 2283; g) A. Ponrouch, C. Frontera, F. Bardé, M. R. Palacin, *Nat. Mater.* **2016**, *15*, 169.
- [4] a) S. J. Richard Prabakar, A. B. Ikhe, W. B. Park, K.-C. Chung, H. Park, K.-J. Kim, D. Ahn, J. S. Kwak, K.-S. Sohn, M. Pyo, *Adv. Sci.* **2019**, *6*, 1902129; b) J. Park, Z.-L. Xu, G. Yoon, S. K. Park, J. Wang, H. Hyun, H. Park, J. Lim, Y.-J. Ko, Y. S. Yun, K. Kang, *Adv. Mater.* **2020**, *32*, 1904411.
- [5] a) S. Kim, L. Yin, M. H. Lee, P. Parajuli, L. Blanc, T. T. Fister, H. Park, B. J. Kwon, B. J. Ingram, P. Zapol, R. F. Klie, K. Kang, L. F. Nazar, S. H. Lapidus, J. T. Vaughey, *ACS Energy Lett.* **2020**, *5*, 3203; b) B. Jeon, J. W. Heo, J. Hyoung, H. H. Kwak, D. M. Lee, S.-T. Hong, *Chem. Mater.* **2020**; c) A. L. Lipson, S. Kim, B. Pan, C. Liao, T. T. Fister, B. J. Ingram, *J. Power Sources* **2017**, *369*, 133.
- [6] a) A. L. Lipson, B. Pan, S. H. Lapidus, C. Liao, J. T. Vaughey, B. J. Ingram, *Chem. Mater.* **2015**, *27*, 8442; b) R. Y. Wang, C. D. Wessells, R. A. Huggins, Y. Cui, *Nano Lett.* **2013**, *13*, 5748.
- [7] M. Cabello, F. Nacimiento, J. R. González, G. Ortiz, R. Alcántara, P. Lavela, C. Pérez-Vicente, J. L. Tirado, *Electrochem. Commun.* **2016**, *67*, 59.
- [8] a) M. Cabello, F. Nacimiento, R. Alcántara, P. Lavela, C. Pérez Vicente, J. L. Tirado, *Chem. Mater.* **2018**, *30*, 5853; b) T. Tojo, H. Tawa, N. Oshida, R. Inada, Y. Sakurai, *J. Electroanal. Chem.* **2018**, *825*, 51.
- [9] M. Liu, Z. Rong, R. Malik, P. Canepa, A. Jain, G. Ceder, K. A. Persson, *Energy Environ. Sci.* **2015**, *8*, 964.
- [10] M. Liu, A. Jain, Z. Rong, X. Qu, P. Canepa, R. Malik, G. Ceder, K. A. Persson, *Energy Environ. Sci.* **2016**, *9*, 3201.
- [11] a) C. Kim, P. J. Phillips, B. Key, T. Yi, D. Nordlund, Y.-S. Yu, R. D. Bayliss, S.-D. Han, M. He, Z. Zhang, A. K. Burrell, R. F. Klie, J. Cabana, *Adv. Mater.* **2015**, *27*, 3377; b) C. Kim, A. A. Adil, R. D. Bayliss, T. L. Kinnibrugh, S. H. Lapidus, G. M. Nolis, J. W. Freeland, P. J. Phillips, T. Yi, H. D. Yoo, B. J. Kwon, Y.-S. Yu, R. Klie, P. J. Chupas, K. W. Chapman, J. Cabana, *Chem. Mater.* **2018**, *30*, 1496; c) X. Sun, P. Bonnicks, V. Duffort, M. Liu, Z. Rong, K. A. Persson, G. Ceder, L. F. Nazar, *Energy Environ. Sci.* **2016**, *9*, 2273; d) P. Bonnicks, L. Blanc, S. H. Vajargah, C.-W. Lee, X. Sun, M. Balasubramanian, L. F. Nazar, *Chem. Mater.* **2018**, *30*, 4683.
- [12] a) L. Hu, J. R. Jokisaari, B. J. Kwon, L. Yin, S. Kim, H. Park, S. H. Lapidus, R. F. Klie, B. Key, P. Zapol, B. J. Ingram, J. T. Vaughey, J. Cabana, *ACS Energy Lett.* **2020**, *5*, 2721; b) B. J. Kwon, K.-C. Lau, H. Park, Y. A. Wu, K. L. Hawthorne, H. Li, S. Kim, I. L. Bolotin, T. T. Fister, P. Zapol, R. F. Klie, J. Cabana, C. Liao, S. H. Lapidus, B. Key, J. T. Vaughey, *Chem. Mater.* **2020**, *32*, 1162.
- [13] R. D. Bayliss, B. Key, G. Sai Gautam, P. Canepa, B. J. Kwon, S. H. Lapidus, F. Dogan, A. A. Adil, A. S. Lipton, P. J. Baker, G. Ceder, J. T. Vaughey, J. Cabana, *Chem. Mater.* **2020**, *32*, 663.
- [14] a) P. Canepa, G. Sai Gautam, D. Broberg, S.-H. Bo, G. Ceder, *Chem. Mater.* **2017**, *29*, 9657; b) P. Canepa, S.-H. Bo, G. Sai Gautam, B. Key, W. D. Richards, T. Shi, Y. Tian, Y. Wang, J. Li, G. Ceder, *Nat.*

- Commun.* **2017**, *8*, 1759; c) J. Koettgen, C. J. Bartel, G. Ceder, *Chem. Commun.* **2020**, *56*, 1952.
- [15] B. L. Cushing, J. B. Wiley, *J. Solid State Chem.* **1998**, *141*, 385.
- [16] H. Park, P. Zapol, *J. Mater. Chem. A* **2020**, *8*, 21700.
- [17] Y. Miyazaki, X. Huang, T. Kajiwara, H. Yamane, T. Kajitani, *J. Ceram. Soc. Jpn.* **2009**, *117*, 42.
- [18] H. Pausch, H. Müller-Buschbaum, *Z. Anorg. Allg. Chem.* **1974**, *405*, 113.
- [19] Y. Takahashi, N. Kijima, K. Tokiwa, T. Watanabe, J. Akimoto, *J. Phys.: Condens. Matter* **2007**, *19*, 436202.
- [20] W. Sun, S. T. Dacek, S. P. Ong, G. Hautier, A. Jain, W. D. Richards, A. C. Gamst, K. A. Persson, G. Ceder, *Sci. Adv.* **2016**, *2*, e1600225.
- [21] a) L. Bindi, E. Sirotkina, A. V. Bobrov, T. Irifune, *J. Phys. Chem. Solids* **2014**, *75*, 638; b) M. Shizuya, M. Isobe, E. Takayama-Muromachi, *J. Solid State Chem.* **2007**, *180*, 2550.
- [22] H. Park, Y. Cui, S. Kim, J. T. Vaughey, P. Zapol, *J. Phys. Chem. C* **2020**, *124*, 5902.
- [23] S. Kim, X. Ma, S. P. Ong, G. Ceder, *Phys. Chem. Chem. Phys.* **2012**, *14*, 15571.
- [24] X. Ma, H. Chen, G. Ceder, *J. Electrochem. Soc.* **2011**, *158*, A1307.
- [25] A. Jain, S. P. Ong, G. Hautier, W. Chen, W. D. Richards, S. Dacek, S. Cholia, D. Gunter, D. Skinner, G. Ceder, K. A. Persson, *APL Mater.* **2013**, *1*, 011002.
- [26] W. Zhang, D.-H. Seo, T. Chen, L. Wu, M. Topsakal, Y. Zhu, D. Lu, G. Ceder, F. Wang, *Science* **2020**, *367*, 1030.
- [27] D. C. Hannah, G. Sai Gautam, P. Canepa, G. Ceder, *Adv. Energy Mater.* **2018**, *8*, 1800379.
- [28] A. Miura, H. Ito, C. J. Bartel, W. Sun, N. C. Rosero-Navarro, K. Tadanaga, H. Nakata, K. Maeda, G. Ceder, *Mater. Horiz.* **2020**, *7*, 1310.
- [29] A. Wustrow, B. Key, P. J. Phillips, N. Sa, A. S. Lipton, R. F. Klie, J. T. Vaughey, K. R. Poeppelmeier, *Inorg. Chem.* **2018**, *57*, 8634.
- [30] A. Van der Ven, G. Ceder, *J. Power Sources* **2001**, *97–98*, 529.
- [31] a) D.-H. Seo, J. Lee, A. Urban, R. Malik, S. Kang, G. Ceder, *Nat. Chem.* **2016**, *8*, 692; b) G. Assat, J.-M. Tarascon, *Nat. Energy* **2018**, *3*, 373; c) D. Kim, M. Cho, K. Cho, *Adv. Mater.* **2017**, *29*, 1701788.
- [32] J. B. Goodenough, Y. Kim, *J. Solid State Chem.* **2009**, *182*, 2904.
- [33] L. Blanc, C. J. Bartel, H. Kim, Y. Tian, H. Kim, A. Miura, G. Ceder, L. F. Nazar, *ACS Mater. Lett.* **2021**, *3*, 1213.
- [34] X. Fu, D. N. Beatty, G. G. Gaustad, G. Ceder, R. Roth, R. E. Kirchain, M. Bustamante, C. Babbitt, E. A. Olivetti, *Environ. Sci. Technol.* **2020**, *54*, 2985.
- [35] M. H. Han, E. Gonzalo, G. Singh, T. Rojo, *Energy Environ. Sci.* **2015**, *8*, 81.
- [36] a) E. A. Olivetti, G. Ceder, G. G. Gaustad, X. Fu, *Joule* **2017**, *1*, 229; b) W. Li, E. M. Erickson, A. Manthiram, *Nat. Energy* **2020**, *5*, 26.
- [37] P. Vassilaras, D.-H. Kwon, S. T. Dacek, T. Shi, D.-H. Seo, G. Ceder, J. C. Kim, *J. Mater. Chem. A* **2017**, *5*, 4596.
- [38] Z. Shadike, Y.-N. Zhou, L.-L. Chen, Q. Wu, J.-L. Yue, N. Zhang, X.-Q. Yang, L. Gu, X.-S. Liu, S.-Q. Shi, Z.-W. Fu, *Nat. Commun.* **2017**, *8*, 566.
- [39] Z. Wang, D. Wang, Z. Zou, T. Song, D. Ni, Z. Li, X. Shao, W. Yin, Y. Wang, W. Luo, M. Wu, M. Avdeev, B. Xu, S. Shi, C. Ouyang, L. Chen, *Natl. Sci. Rev.* **2020**, *7*, 1768.
- [40] P. Hohenberg, W. Kohn, *Phys. Rev.* **1964**, *136*, B864.
- [41] G. Kresse, J. Furthmüller, *Phys. Rev. B* **1996**, *54*, 11169.
- [42] a) P. E. Blöchl, *Phys. Rev. B* **1994**, *50*, 17953; b) G. Kresse, D. Joubert, *Phys. Rev. B* **1999**, *59*, 1758.
- [43] J. P. Perdew, K. Burke, M. Ernzerhof, *Phys. Rev. Lett.* **1996**, *77*, 3865.
- [44] L. Wang, T. Maxisch, G. Ceder, *Phys. Rev. B* **2006**, *73*, 195107.
- [45] S. P. Ong, W. D. Richards, A. Jain, G. Hautier, M. Kocher, S. Cholia, D. Gunter, V. L. Chevrier, K. A. Persson, G. Ceder, *Comput. Mater. Sci.* **2013**, *68*, 314.
- [46] Y. Shimakawa, T. Numata, J. Tabuchi, *J. Solid State Chem.* **1997**, *131*, 138.
- [47] a) S. P. Ong, L. Wang, B. Kang, G. Ceder, *Chem. Mater.* **2008**, *20*, 1798; b) A. Jain, G. Hautier, S. P. Ong, C. J. Moore, C. C. Fischer, K. A. Persson, G. Ceder, *Phys. Rev. B* **2011**, *84*, 045115.
- [48] G. Henkelman, B. P. Uberuaga, H. Jónsson, *J. Chem. Phys.* **2000**, *113*, 9901.